Computational Kinetics Simulation of Precipitation and Dissolution of Gamma Prime (γ') in Heat Treating and Welding of 718plus Superalloy

BO WANG, FAN ZHANG, WEISHENG CAO, SHUANGLIN CHEN, and SINDO KOU

The evolution of the strengthening precipitate in a precipitation-hardening alloy, such as the gamma prime (γ') phase in Ni-base superalloys, during heat treating and welding can affect the resultant mechanical properties significantly. Computational kinetics simulation can be a useful tool for understanding and controlling of such evolution. The present study was conducted to simulate the γ' precipitation and dissolution during aging and welding of the recently developed Ni-base superalloy 718plus using *the PanPrecipitation* module of the *Pandat* software along with available thermodynamic and kinetic databases. The purpose was to demonstrate the application of such software and databases to materials processing including heat treating and welding. The variations in the volume fraction, average precipitation size, and number density of γ' with time during aging and welding were calculated. The calculated results under aging condition agreed well with the available experimental data, while those under welding also predicted the correct trend.

DOI: 10.1007/s11661-014-2617-2

I. INTRODUCTION

NICKEL-BASED superalloys have been extensively used for high-temperature applications such as jet engines, gas turbines, and nuclear reactors. Allvac® 718plus™ alloy[1] is a recently developed Ni-base superalloy which is strengthened by ordered face-centered cubic (fcc) intermetallic γ' phase. It was developed to raise the working temperature range of its baseline superalloy, 718, from 923 K to 973 K (650 °C to 700 °C), while maintaining the workability of alloy 718. It is considered to be weldable as compared to other Ni-base superalloys strengthened by the γ' phase.[2]

The evolution of the γ' phase during heat treating of Ni-base superalloys has been studied, for instance, its precipitation and dissolution in Udimet 520[3] and its precipitation in alloy 718plus.[4–10] The precipitation behavior and mechanical properties of alloy 718plus were studied by Zickler *et al.*[5] as a function of aging temperature and time by hardness testing, electron microscopy, atom probe tomography, and *in situ* high-temperature small-angle neutron scattering. The radius R, number density N, and volume fraction f of γ' precipitates as a function time at various aging temperatures were determined. Their data will be used in the present study.

The evolution of the γ' phase in Ni-base superalloys during welding has also been studied, for instance, its solution and reprecipitation in the HAZ of Udimet 700.[8] The liquid formation (called liquation) and cracking in the partially melted zone has been studied for 718plus.[2,10] However, the dissolution and reprecipitation of γ' in the HAZ, which is important in understanding the cracking, have not been studied for this alloy.

The present work aims at understanding the γ' evolution in alloy 718plus during heat treating and welding using a computational approach. The volume fraction, average precipitation size, and number density of γ' will be calculated as a function of time using the *PanPrecipitation* module of *Pandat*™ software[11] and corresponding thermodynamic and kinetic databases. The purpose is to demonstrate the application of such software and databases to materials processing including heat treating and welding.

II. NUMERICAL MODEL

Precipitation can be a complex process involving the simultaneous occurrence of nucleation, growth, and coarsening. Accurate modeling of such a process requires a synchronous consideration of all these contributions in order to simulate the temporal evolution of microstructure and further predict the corresponding responses of mechanical properties. In the present study, an integrated computational tool, *PanPrecipitation* of software *Pandat*[11] was used to simulate the γ' dissolution and precipitation kinetics in alloy 718plus during

BO WANG, Professor, is with the Shanghai Key Laboratory of Modern Metallurgy and Materials Processing, School of Materials Science and Engineering, Shanghai University, Shanghai 200072, P.R. China. Contact e-mail: bowang@shu.edu.cn FAN ZHANG, President, WEISHENG CAO and SHUANGLIN CHEN, Vice presidents, are with the CompuTherm LLC, 437 S. Yellowstone Dr., Madison WI 53719. SINDO KOU, Professor, is with the Department of Materials Science and Engineering, University of Wisconsin-Madison, Madison, WI 53705.

Manuscript submitted December 19, 2013.
Article published online October 17, 2014

aging and welding. This model tool consists of three separate modules dealing with: (1) thermodynamic/mobility calculation based on the Calphad method, (2) simulation of microstructure using the built-in precipitation models, and (3) prediction of mechanical properties according to developed age hardening models.[12]

In the integrated workspace, the *PanPrecipitation* module is fully coupled with the automatic thermodynamic calculation engine, *PanEngine*.[11] Therefore, the thermodynamic properties and atomic mobility data needed for precipitation simulation can be obtained instantly from *PanEngine* during the simulation.

PanPrecipitation has three built-in precipitation models for microstructure simulation at multi-levels: 1. the well-known JMAK model (Johnson–Mehl–Avrami–Kolmogorov) for estimation of the overall transformation rate, 2. the Fast-Acting model based on Langer and Schwartz theory[13] for simulation of the evolution of particle number density and mean size, and 3. the more advanced KWN (Kampmann & Wagner Numerical) model[14,15] for prediction of the full evolution of the particle size distribution (PSD) in addition to average quantities. The microstructure information obtained (*e.g.*, volume fraction, number density, mean size, and PSD) can then be used to predict the age hardening behavior on the basis of the proposed strengthening models.

In order to simulate the nucleation, growth and coarsening of γ' in multi-component and multi-phase alloys such as superalloys, the fast-acting model based on the theory of Langer and Schwartz will be adopted here.[13] This theory is derived from the classical nucleation and growth theory that has been used to describe nucleation and growth, including the evolution of the particle number density and mean size.

A. *Nucleation*

In the precipitation stage, we consider simultaneously nucleation and growth. The variation of the precipitation density is given by the nucleation rate, and the evolution of the mean precipitate radius is given by combining the growth of existing precipitates and the arrival of new precipitates at the nucleation radius R^*.

According to the classical nucleation theory,[13] the homogeneous nucleation rate is as follows:

$$I = N_v Z \beta^* \exp\left(-\frac{4\pi\gamma r^{*2}}{3kT}\right) \exp\left(-\frac{\tau}{t}\right), \qquad [1]$$

where N_v is the number of nucleation sites per unit volume, Z is the Zeldovich factor (which accounts for the decay of some of the supercritical clusters), β^* is the frequency factor, γ is the interfacial energy of the nucleus (which is assumed to be isotropic and size independent), r^* is the critical radius that a cluster must reach to become a nucleus, and τ is the incubation time for nucleation (the time needed to establish the initial cluster distribution). k is the Boltzmann constant, and T is temperature in degree Kelvin.

The critical radius depends on the driving force for transformation and the interfacial energy. Ignoring the strain energy, the critical radius can be written as

$$r^* = \frac{-2\gamma}{\Delta G_v}, \qquad [2]$$

where ΔG_v is the chemical volume free energy change driving nucleation. Assuming a spherical nucleus, Z, β^*, and τ can be determined as follows:

$$Z = \frac{V_\alpha \Delta G_v^2}{8\pi\sqrt{\gamma^3 kT}}, \qquad [3]$$

$$\beta^* = \frac{16\pi\gamma^2 cD}{\Delta G_v^2 a^4}, \qquad [4]$$

$$\tau = \frac{8kT\gamma a^4}{V_\alpha^2 \Delta G_v^2 Dc}, \qquad [5]$$

where V_α is the volume per atom in the matrix, c is the concentration (atomic fraction) of solute in the matrix, a is the lattice constant of the product phase, and D is the diffusivity of the solute in the matrix.

For the multi-component system, these parameters have been proposed by Kozeschnik *et al.*[16] and implemented in PanPrecipitation.[17] In this simulation, the values of the diffusivities and driving force come from the thermodynamic and kinetic database of PANDAT software.

B. *Growth*

Experimental investigations from the Reference 5 showed that the Nickel-based 718plus superalloy contained nanometer-sized spherical γ' phase precipitates in the γ matrix. Therefore, precipitates are assumed spherical in morphology, with their growth controlled by the rate at which solute atoms can diffuse to the spherical particles. In this case, the growth rate is given as follows[15]:

$$\frac{dr}{dt} = \frac{D}{r}\frac{c_i - c_r^\alpha}{c^\beta - c_r^\alpha}, \qquad [6]$$

where r is the particle radius, c_r^α is the concentration of solute in the α matrix at the interface, and c^β is the concentration of solute in the β precipitates. c_r^α is calculated from c_∞^α the equilibrium concentration of solute in the α matrix for a planar interface using the following Gibbs–Thomson equation:

$$c_r^\alpha = c_\infty^\alpha \exp\left(\frac{2\gamma V_m}{R_g T}\frac{1}{r}\right), \qquad [7]$$

where V_m is the molar volume of the precipitating phase, γ is the interfacial energy of the growing (or shrinking) particle. The growth of heterogeneously nucleated particles is treated in the same way as growth for homogeneously nucleated particles. The value of the interfacial energy used was 0.047 J m^{-1}, taken from the experimentally determined value of Zickler's data.[5] The value of the molar volume for the gamma prime (γ') precipitation phase was 7.1×10^{-6} in this simulation.

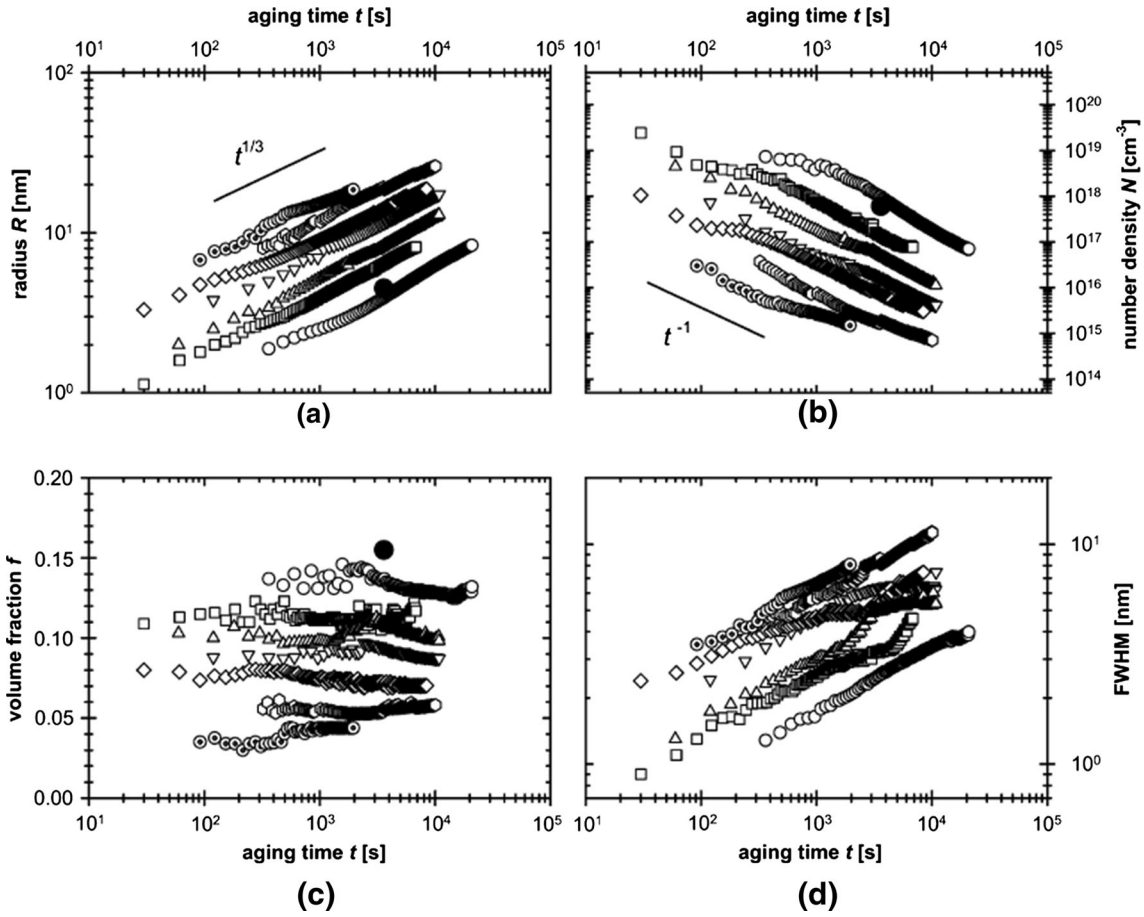

Fig. 1—Radius R (*a*), number density N (*b*), volume fraction f (*c*), and full width at half maximum (FWHM) of the particle size distribution (*d*) of γ' precipitates in alloy 718plus determined by SANS (open symbols) and API (filled symbols), respectively, as a function of aging time t at various temperatures: 1048 K (775 °C) (circles), 1073 K (800 °C) (squares), 1098 K (825 °C) (triangles up), 1123 K (850 °C) (triangles down), 1148 K (875 °C)(diamonds), 1173 K (900 °C) (hexagons), and 1198 K (925 °C) (dotted circles).[5]

Table 1. Chemical Composition (Weight Percent) of Alloy 718plus[5]

Alloy	Ni	Ti	Al	Nb	Cr	Co	Fe	Mo	W	C
718plus	base	0.73	1.42	5.55	18.02	9.11	9.51	2.66	1.05	0.021

III. RESULTS OF AGING SIMULATION AND DISCUSSION

Before presenting the calculated results, the experimental work by Zickler *et al.*[5] is first described as follows. The composition of the alloy 718plus used is shown in Table 1. The samples were solution-treated (homogenized) at 1283 K (1010 °C) for 7200 seconds in a furnace and then immediately water quenched. They were isothermally aged in ambient atmosphere at 1048 K, 1098 K, 1148 K, 1173 K, 1198 K, and 1223 K (775 °C, 825 °C, 875 °C, 900 °C, 925 °C, and 950 °C).

Atom probe tomography and electron microscopy were used for microstructural characterization of the aged samples. Small-angle neutron scattering method was performed to study the precipitation kinetics of the γ' phase. Figure 1 shows the radius R, number density N, and volume fraction f of γ' phase precipitates as a function time t at various aging temperatures T.[5] These data will be used to check the validity of the calculated results subsequently.

Figure 2 shows the calculated particle number density N of γ' precipitates as a function of the aging time t at 1048 K, 1148 K, and 1198 K (775 °C, 875 °C, and 925 °C). As shown, shortly after coarsening starts, the number density of γ' precipitates decreases at all temperature with increasing aging time. The calculated results agree well with the experimental results of Zickler *et al.*[5]

Figure 3 shows the calculated particle radius R of γ' precipitates *vs* the aging time t at the same temperatures. It can be seen that R increases with increasing aging time. The calculated results again agree well with the experimental results of Zickler *et al.*[5]

Figure 4 shows the calculated volume fraction f of γ' precipitates against the aging time t at the same temperatures. As shown, the volume fraction of γ' precipitates increases initially but levels off with further

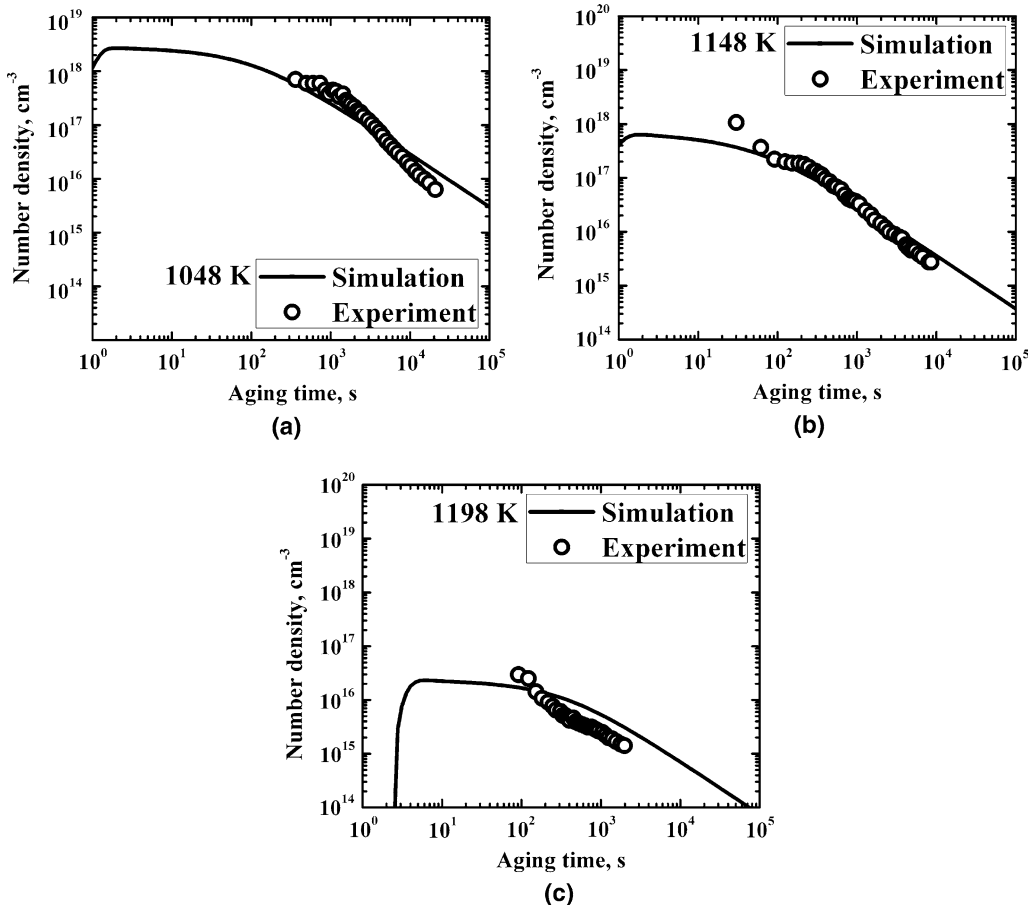

Fig. 2—Comparison of calculated particle number density N at aging temperatures 1048 K (775 °C) (*a*), 1148 K (875 °C) (*b*), and 1198 K (925 °C) (*c*) with experimental results of Zickler *et al.*[5]

increase in aging time after coarsening starts. The calculated volume fraction is higher than the observed one. It is not clear if this difference is caused by δ precipitation.

IV. RESULTS OF WELDING SIMULATION AND DISCUSSION

γ' precipitates in Ni-base superalloys can be dissolved partially or even completely in the HAZ during welding, depending on the alloy composition and the thermal cycles experienced by the heat-affected zone (HAZ) of the weld. A thermal cycle at a specific location in the HAZ is the temperature experienced by the material at the location during welding. It depends on the location, the heat input, the material and dimensions of the workpiece, and the backing plate. The heat input in turn depends on the welding current, voltage, speed, and process.

A. *Welding Thermal Cycles*

Thermal cycles in the HAZ are often measured with thermocouples. However, in the case of electron-beam welding, the HAZ is too narrow and the temperature changes too fast for thermocouples. Consequently, they need to be calculated. Thermal cycles can be calculated by analytical equations. In order to take into account the latent heat of fusion and the power-density distribution of the heat source, however, computer modeling was used instead. For simplicity, heat transfer in the workpiece was assumed by conduction. That is, fluid flow in the weld pool was neglected as it is affected by the complicated interactions between the vapor pressure, gravity and surface tension to establish the keyhole. The effect of the keyhole was considered using a volumetric heat source that has a Gaussian distribution at the workpiece surface and that decays linearly in the z-direction (that is, below the surface). Since the temperature dependence of the thermophysical properties of alloy 718plus is not readily available, the properties are assumed constant. The heat transfer coefficient at the top surface of the workpiece was also assumed constant.

Figure 5 is a schematic illustration of electron-beam welding. The heat source, that is, the electron beam, and the origin of the coordinate system (x, y, and z) are both stationary, while the workpiece travels at a constant speed u in the x-direction. A vertical plane cutting normal to the welding direction reveals the transverse cross-section of the resultant weld. Except for the initial

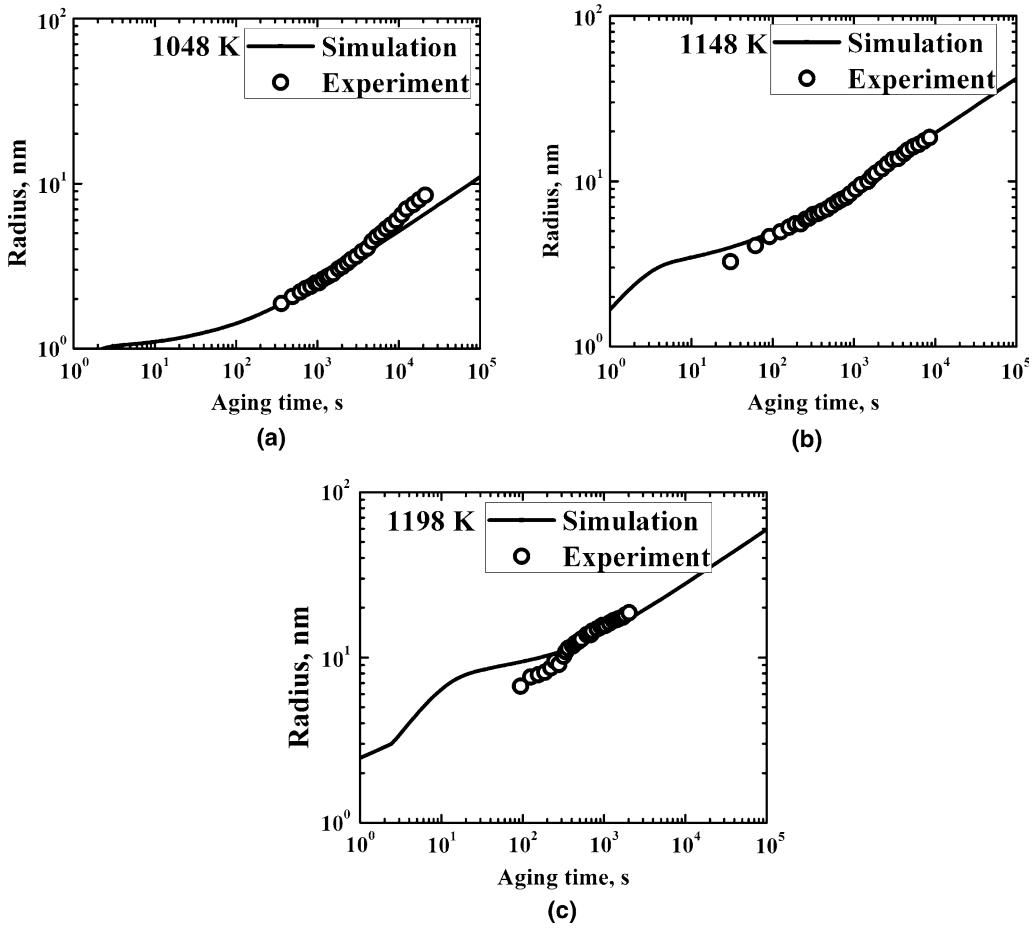

Fig. 3—Comparison of calculated particle radius R at aging temperatures 1048 K (775 °C) (*a*), 1148 K (875 °C) (*b*), and 1198 K (925 °C) (*c*) with experimental results of Zickler *et al.*[5]

and final transients of welding, heat flow in a workpiece of sufficient length is steady, or quasi-stationary, with respect to the moving heat source. Thus, the temperature dependence on time can be neglected.

With the above assumptions, the energy equation can be written as

$$\nabla \cdot (k\nabla T) - \rho c u \frac{\partial T}{\partial x} + Q_0 = 0, \qquad [8]$$

where u is the welding speed (m/s), T is temperature (K), k is the workpiece thermal conductivity (W/m K), ρ is the density of workpiece (kg/m^3), c is the heat capacity (J/kg K), and Q_0 is the heat source term. Q_0 consists of two parts: 1. the latent heat due to melting and solidification ($q_L = \rho L \frac{\partial f_s u}{\partial x}$, where L is the latent heat of fusion andf_s the fraction of solid), and 2. the welding heat source (q_{in}).

The input heat source was assumed Gaussian as follows:

$$q_{in} = \frac{3Q}{\pi a^2} \exp\left[\frac{r^2}{-a^2/3}\right], \qquad [9]$$

where q_{in} is the power density, Q is the rate of heat transfer from the heat source to the workpiece, and a is the effective radius of the heat source.

The boundary conditions are as follows. At the central plane ($y = 0$), $\frac{\partial T}{\partial y} = 0$. On the top surface, heat losses by convection were considered. Since all other surfaces of the workpiece are far away from the electron beam, they were set at 298 K (25 °C). The initial temperature of workpiece before welding was 298 K (25 °C). The energy equation was discretized for the use of the finite-difference method. The grid was non-uniform, being finer near the heat source and coarser away from it.

The 718plus workpiece was 12 by 12 by 100 mm, solution heat-treated before welding specimens, and welded the 100 mm direction by electron-beam welding at 44 kV voltage, 79 mA beam current, and 152 cm/min welding speed.[2] The calculated shape of the fusion zone is shown in Figure 6, along with the observed transverse cross-section of the weld.[2] The calculated fusion-zone shape agrees well with the observed one.

The calculated weld thermal cycles are shown in Figure 7 for three different locations in the HAZ of alloy 718plus. Locations 1, 2, and 3 are at $y = 0.475$, 0.525, and 0.575 mm, respectively, and at $z = 4.0$ mm. At $z = 4.0$ mm, the calculated fusion boundary was at $y = 0.45$ mm, and thus the distances from the fusion boundary to Locations 1, 2, and 3 in the y-direction were 0.05, 0.1, and 0.15 mm, respectively. According to

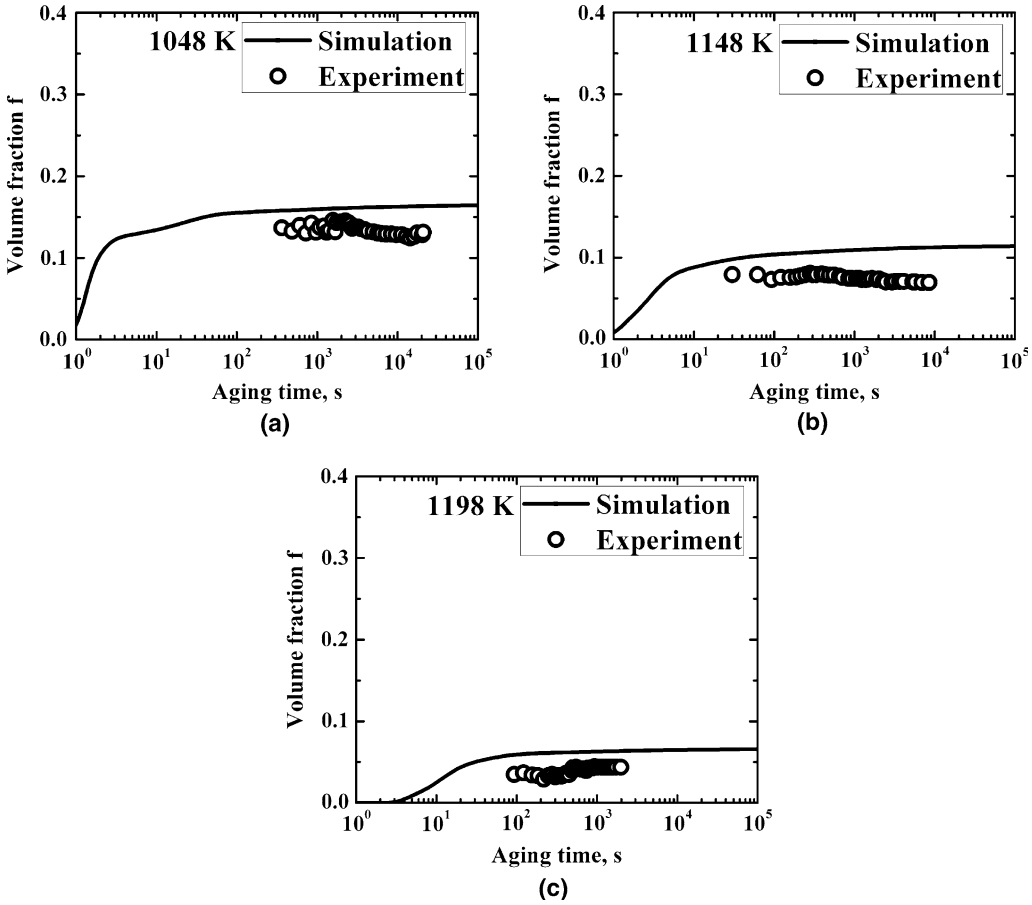

Fig. 4—Comparison of calculated volume fraction f of γ' precipitates at aging temperatures 1048 K (775 °C) (*a*), 1148 K(875 °C) (*b*), and 1198 K (925 °C) (*c*) with experimental results of Zickler *et al.*[5]

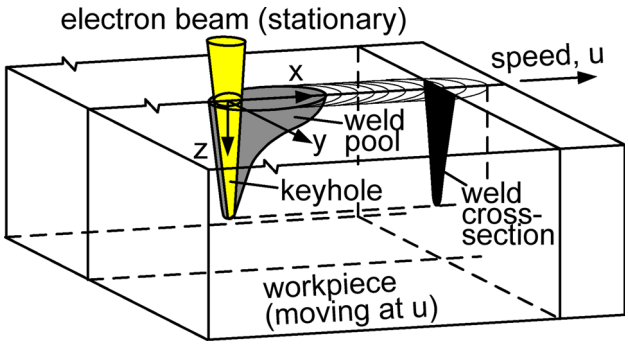

Fig. 5—Schematic illustration of electron-beam welding.

the calculated thermal cycles, the peak temperatures at Locations 1, 2, and 3 are 1495 K, 1383 K, and 1288 K (1222 °C, 1110 °C, and 1015 °C), respectively. Thus, the closer to the fusion boundary, the higher the peak temperature becomes.

B. *Dissolution and Precipitation in HAZ*

The γ' dissolution and precipitation in the HAZ during the welding of alloy 718plus were again simulated using software *PanPrecipitation* and the same

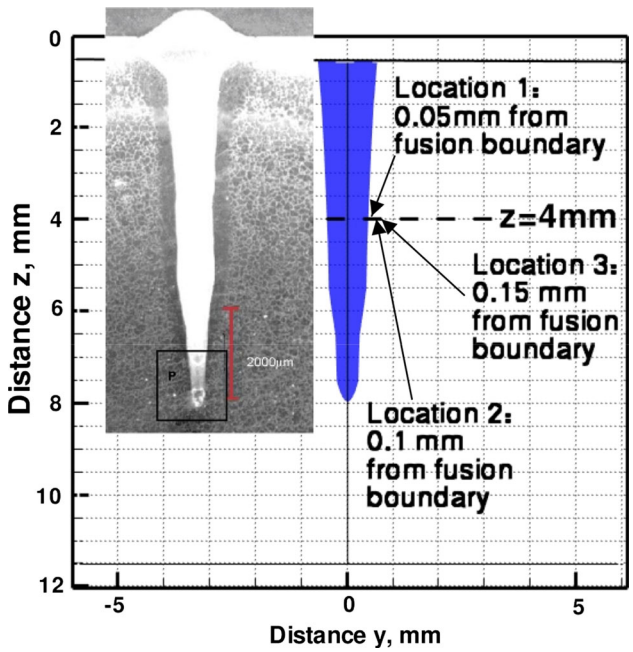

Fig. 6—Comparison of experimental and simulated results for fusion zone profile in EBW. The location of thermal cycles are shown by the crosses.

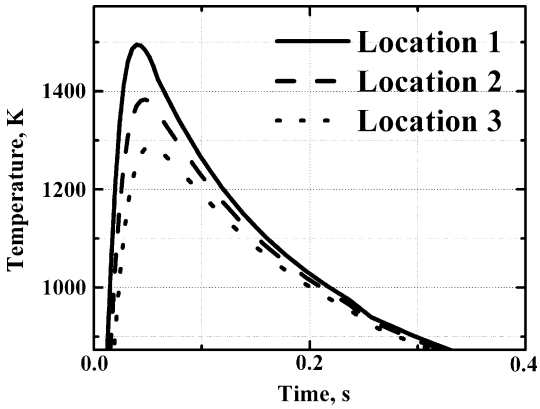

Fig. 7—Thermal cycles in the HAZ.

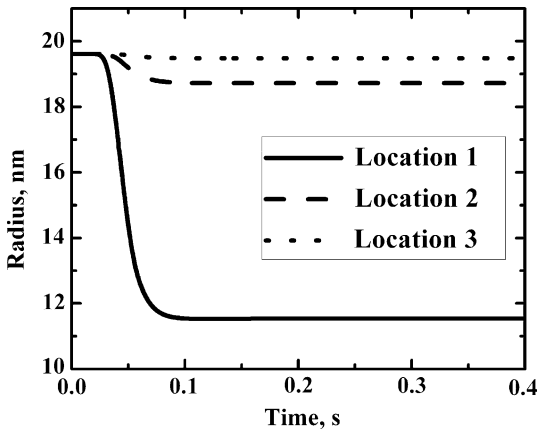

Fig. 8—Effect of thermal cycle peak temperature on the average size of γ'.

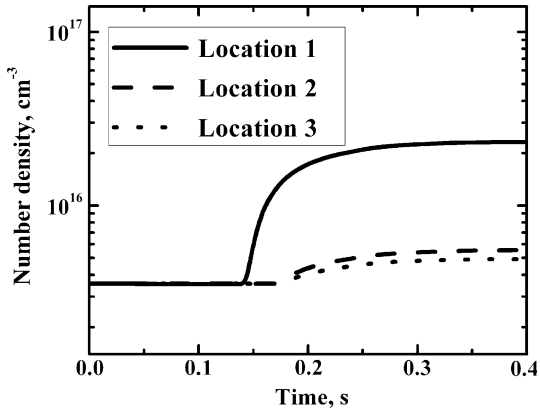

Fig. 9—Effect of thermal cycle peak temperature on the number density of γ'.

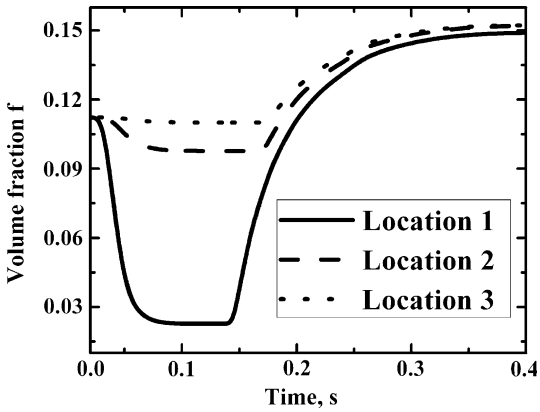

Fig. 10—Effect of thermal cycle peak temperature on the volume fraction of γ'.

thermodynamic and kinetic databases as in the case of heat treating. However, the temperature at a given location in the HAZ was not kept constant as in heat treating but allowed to vary with time according the thermal cycle calculated at that location.

The effect of the thermal cycle on the dissolution and precipitation of the γ' phase in the HAZ is shown in Figures 8 through 10. Figure 8 shows the effect of the thermal cycle on the average radius of γ' precipitates. The precipitates dissolve upon heating, causing their average radius to decrease. This continues somewhat beyond the peak temperature. The average radius then remains constant upon further cooling. The higher the peak temperature of the thermal cycle is, the more γ' dissolution.

The effect of the thermal cycle on the number density of γ' precipitates is shown in Figure 9. The number density seems to increase during cooling through the temperature range of about 1173 K to 1073 K (900 °C to 800 °C). The higher the peak temperature is, the more significantly the number density increases.

The effect of the thermal cycle on the volume fraction of γ' precipitates is shown in Figure 10. The initial decrease in the volume fraction is associated with the dissolution of the precipitates upon heating. The higher the peak temperature in the HAZ is, the lower the fraction of precipitates. The volume fraction remains at the minimum for a period of about 0.1 second. After that, it increases with time because of the increase in the number density of the precipitates with time.

It is well known that the heat treating condition of the workpiece before welding can affect the HAZ microstructure and properties significantly. The effect of preweld heat treating on γ' precipitates in the HAZ can be studied by combining the simulation of the heat treating with that of welding.

V. CONCLUSIONS

1. The precipitation kinetics of the γ' phase during the aging of Ni-base alloys has been simulated using the *PanPrecipitation* software and Ni-based superalloy thermodynamic and kinetic databases of

CompuTherm. The calculated results agree well with the experimental results of 718plus superalloy.
2. The dissolution and reprecipitation kinetics of the γ' phase in the HAZ of Ni-base superalloys during welding have also been simulated using the same software and databases. The significant effect of the thermal cycle on the kinetics has been demonstrated.
3. The present study has demonstrated that these software package and databases can be a useful tool for studying the evolution of γ' precipitates in heat treating and welding of Ni-base superalloys and the effect of pre-weld heat treating on γ' precipitates in the HAZ of the resultant weld.

ACKNOWLEDGMENTS

The first author gratefully acknowledges the financial support received from the Innovative Foundation of Shanghai University (SDCX2013031). This work was also supported by the National Science Foundation under Grant No. IIP-1034695 and the University of Wisconsin Foundation through the Industry/University Collaborative Research Center (I/UCRC) for Integrated Materials Joining Science for Energy Applications. All calculations were performed using the *PanPrecipitation* and *PanEngine* of *Pandat*^{TM} software licensed from CompuTherm LLC, USA.

REFERENCES

1. W.D. Cao, U.S. Patent 6730.254 B2, 2004.
2. K.R. Vishwakarma, N.L. Richards, and M.C. Chaturvedi: *Mater. Sci. Eng., A*, 2008, vol. 480, pp. 517–28.
3. M. Jahazi and A.R. Mashreghi: *Mater. Sci. Eng.*, 2002, vol. 18, pp. 458–62.
4. W.-D. Cao: in *Superalloy 718, 625, 706 and Derivatives 2005*, E.A. Loria, ed., TMS, 2005. pp. 165–77.
5. G.A. Zickler, R. Schnitzer, R. Radis, R. Hochfellner, R. Schweins, M. Stockinger, and H. Leitner: *Mater. Sci. Eng., A*, 2009, vol. 523, pp. 295–303.
6. L. Whitmore, H. Leitner, E. Povoden-Karadeniz, R. Radis, and M. Stockinge: *Mater. Sci. Eng. A*, 2012, vol. 534, pp. s413–23.
7. R. Radis, G.A. Zickler, M. Stockinger, C. Sommitsch, and E. Kozeschnik: *Mater. Sci. Forum*, 2010, vols. 638–642, pp. 2712–17.
8. W.A. Owczarski and C.P. Sullivan: *Weld. J.*, 1964, vol. 43, pp. 393s–99s.
9. B. Radhakrishnan and R.G. Thompson: *Metall. Trans. A*, 1993, vol. 24A, pp. 2773–85.
10. O.A. Idowu, O.A. Ojo, and M.C. Chaturvedi: *Weld. J.*, 2009, vol. 88, pp. 179s–87s.
11. Pandat, PanPrecipitation and PanEngine are trademarks of CompuTherm software. http://www.computherm.com/.
12. W. Cao, F. Zhang, S.-L. Chen, C. Zhang, and Y.A. Chang: *JOM*, 2011, vol. 63, pp. 29–34.
13. J. Langer and A. Schwartz: *Phys. Rev. A*, 1980, vol. 21 (3), pp. 948–58.
14. R. Kampmann and R. Wagner: in *Decomposition of Alloys: the Early Stages*, P. Haasen, ed., Pergamon Press, Oxford, 1984, pp. 91–105.
15. J.D. Robson: *Mater. Sci. Eng.*, 2004, vol. 20, pp. 441–48.
16. E. Kozeschnik, I. Holzer, B. Sonderegger: *J. Phase Equilib. Diffus.*, 2007, vol. 28(1), pp. 64–71.
17. W. Cao, S.-L. Chen, F. Zhang, K. Wu, Y. Yang, Y.A. Chang, R. Schmid-Fetzer, and W.A. Oates: *CALPHAD*, 2009, vol. 33, pp. 328–42.